ADVANCED ELECTRONIC MATERIALS
www.advelectronicmat.de

Schottky Diode with Asymmetric Metal Contacts on WS_2

*Jihoon Kim, A. Venkatesan, Nhat Anh Nguyen Phan, Yewon Kim, Hanul Kim, Dongmok Whang, and Gil-Ho Kim**

Diode characteristics of transition metal dichalcogenides are studied extensively owing to their electrical and optical properties. In particular, the Schottky barrier diode (SBD) structure has advantages, such as its small leakage current and power consumption, over conventional p–n diodes. This study develops an SBD system using n-type tungsten disulfide (WS_2). By depositing a low work function In (Φ_{In} = 4.1 eV) and high work function Au (Φ_{Au} = 5.1 eV) on n-type WS_2, the diode characteristics are demonstrated to be close to an ideal diode. The In–Au contacts are measured, and SBD characteristics are confirmed with a 1.02 ideality factor at a zero back-gate voltage at room temperature and a rectification ratio up to 5×10^2, even at a low temperature (77 K), indicating almost ideal diode properties. In addition, the In electrodes exhibited improved electrical properties, with a high on/off ratio of 10^7, mobility that is 100 times higher, and Schottky barrier height that is 20 times lower than that of Au electrodes.

1. Introduction

Owing to the urgent need to resolve scaling problems in electronics, transition metal dichalcogenides (TMDs) have been considered next-generation semiconductor materials with their appropriate bandgaps, inherent mobility, and optically ultralow thickness.[1–5] TMD devices can be fabricated in atomic layers, and novel properties can be obtained by stacking several 2D material layers, changing the physical properties depending on the structure.[6,7] Thus, they have attracted much attention in the field of electronics for various applications such as optoelectronics,[8,9] spintronics,[10,11] valleytronics,[12,13] and solar cells.[14] In particular, the application of TMD diodes to switching devices, detectors, and light-emitting diodes has been extensively studied by stacking two types (p- and n-type) of materials and forming depletion regions to rectify the unidirectional current or by doping.[15–19] Conventionally, the diode characteristics are confirmed by combining two materials that have different characteristics for applications such as p–n diodes. However, the bonding of two materials with other structures directly exposes the properties of the 2D material to changes in the external environment, worsening the diode performance compared to that of the original material.

Schottky barrier diode (SBD) is the structure without stacking and combining different materials. It has better power consumption than p–n diodes because of its fast response and low voltage drop in the forwarding region.[20] Recently, remarkable diode characteristics without heterostructures or doping have been reported in the molybdenum disulfide and molybdenum ditelluride SBD structure using only the different metal contacts with work function modulation.[21,22] However, these diodes, which utilize the work function, did not show better ideality factors than the other p–n heterojunction diodes. In this study, unlike previous works, a tungsten disulfide (WS_2) SBD device was fabricated as an ideal-like diode by depositing two different metals. An ideality factor of 1.02 at a zero-gate voltage and rectification ratio of up to 5×10^2 even at different temperatures was obtained by depositing two different metals. WS_2 has a direct bandgap of 2.1 eV in the monolayer and an indirect bandgap of 1.4 eV in the few layers, which is a relatively large bandgap.[23] This results in a wide-wavelength photoreaction and a high absorbance potential for photocatalysis and photodetectors.[24,25] Metallic In and Au made contact with an exfoliated n-type WS_2 flake. In general, n-type materials are familiar with low work function metals because the Fermi level of low work function metals aligned close to the conduction band of the 2D materials will promote electron injection.[26] By contrast, high work function metals with the Fermi level aligned close to the valence band of n-type materials will result in the formation of potential barriers, impeding electron flow. Therefore, metal contacts with WS_2 were fabricated using In for the forward direction and Au for the reverse direction, which corresponds to a lower (Φ_{In} = 4.1 eV) and higher work function (Φ_{Au} = 5.1 eV), respectively. When the In–Au contact was measured, the characteristics of the rectifier diode were confirmed by the difference in the metal work function. We also compared the electrical properties and charge

J. Kim, A. Venkatesan, N. A. N. Phan, Y. Kim, G.-H. Kim
Department of Electrical and Computer Engineering
Sungkyunkwan University (SKKU)
Suwon 16419, Republic of Korea
E-mail: ghkim@skku.edu

H. Kim, D. Whang, G.-H. Kim
Samsung-SKKU Graphene Center
Sungkyunkwan Advanced Institute of Nanotechnology (SAINT)
Sungkyunkwan University (SKKU)
Suwon 16419, Republic of Korea

D. Whang
Department of Advanced Materials Science and Engineering
Sungkyunkwan University (SKKU)
Suwon 16419, Republic of Korea

The ORCID identification number(s) for the author(s) of this article can be found under https://doi.org/10.1002/aelm.202100941.

DOI: 10.1002/aelm.202100941

transfer at the interface of each metal, such as the mobility and Schottky barrier height (SBH) at different temperatures. This can be applied as the simplest SBD without complicated structures and processes such as p–n junctions.

2. Results and Discussion

The WS_2 SBD device is shown schematically in **Figure 1**a. The optical image of the device is shown in Figure 1b, where the five-layer WS_2 is in contact with the Au electrodes on the bottom and the In electrodes on the top side. First, the Au bottom electrodes were prepared on a precleaned Si/SiO_2 wafer (Figure S1a, Supporting Information). Owing to the poor adhesion of Au on SiO_2, a 10 nm thick In adhesion layer was deposited before the deposition of Au, followed by a 30 nm thick Au layer. The dry transfer method was then applied in argon gas for moving the WS_2 flake. Following the transfer of WS_2 on the Au electrodes shown in Figure S1b of the Supporting Information, the In electrode (In/Au) was deposited (Figure S1c, Supporting Information). Figure 1c shows the Raman spectra of the WS_2 flake obtained using a 532 nm laser at room temperature. In the WS_2 Raman spectrum, the presence of signature peaks E^1_{2g} showing the in-plane vibration of atoms and A_{1g} showing out-of-plane directions of S atoms at frequencies of 350 and 415 cm^{-1} confirms that the flake is WS_2 multilayers.[27] The thickness of the WS_2 flake was confirmed by atomic force microscopy (AFM), as shown in Figure 1d. The thickness of the WS_2 flake was 4.8 nm, ensuring that the WS_2 flake was approximately five layers.[28]

The I_D–V_D characteristics using asymmetric In and Au electrodes exhibit marked rectification behavior depending on gate voltages from 0 to 60 V, especially at a high positive gate bias voltage with a rectification ratio of 5×10^2, as shown in **Figure 2**a. Because of the high work function metal (Φ_{Au} = 5.1 eV), Au electrodes making contact with n-type WS_2 form Schottky contact with high SBH in the reverse direction of the diode. By contrast, In electrodes with a low work function (Φ_{In} = 4.1 eV) form an Ohmic-like junction with WS_2 in the forward direction of the diode detailed in Figure 2e. Under the drain voltage, the potential barrier height between the Au and WS_2 sides becomes too high for a considerable amount of current to flow through the metal–semiconductor junction compared with In, and it exhibits the characteristics of the rectification behavior of a classic diode. Figure 2b shows the variation of the I_D–V_G characteristics of the asymmetric In–Au contacts with the different drain voltages. The I_D–V_G characteristics of WS_2 show excellent n-type properties as the transfer characteristics increase with higher drain voltages at room temperature and even at 77 and 400 K (Figure S2b,d, Supporting Information). The WS_2 SBD also exhibited excellent rectifying characteristics, at a zero-gate voltage, for a wide range of operating temperatures (77–400 K). In particular, even in the absence of a gate voltage, the forward to reverse bias current ratio is as

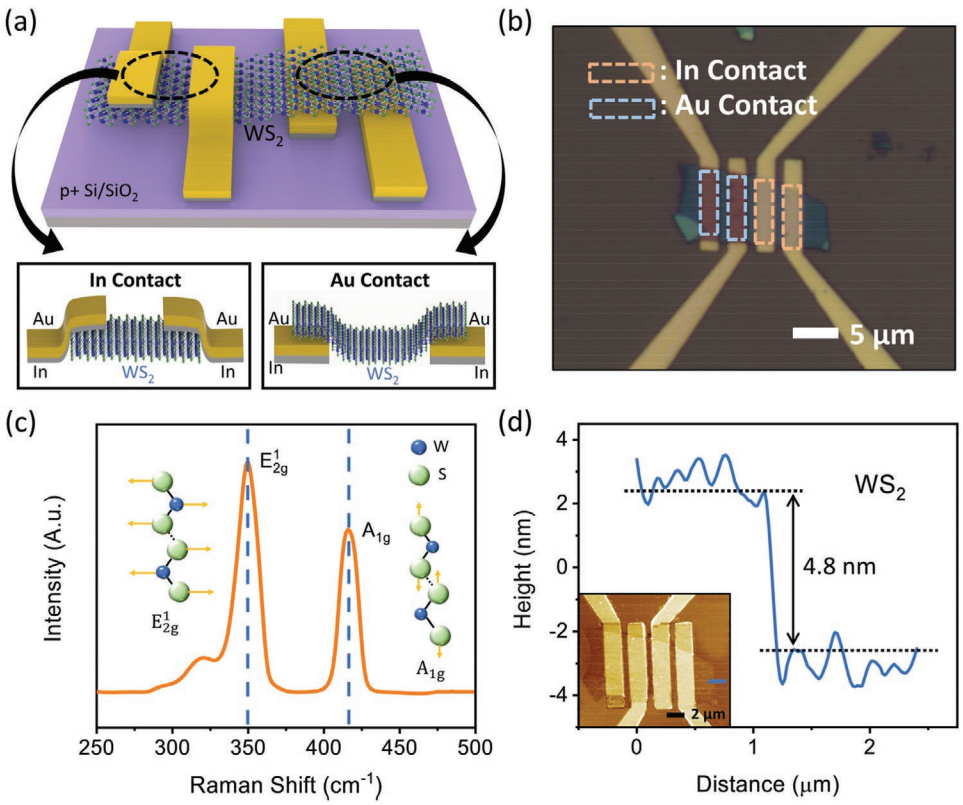

Figure 1. a) Schematic diagram of the WS_2 SBD device and partially enlargement of Au with bottom contacts and In with top contacts. b) Optical image of the WS_2 SBD device with different metal contacts. c) Raman spectrum of WS_2 with atomic displacements showing in-plane and out-of-plane vibrational modes. d) Thickness of the five-layer WS_2. Inset: Atomic force microscopy image with line scan (blue line) of WS_2.

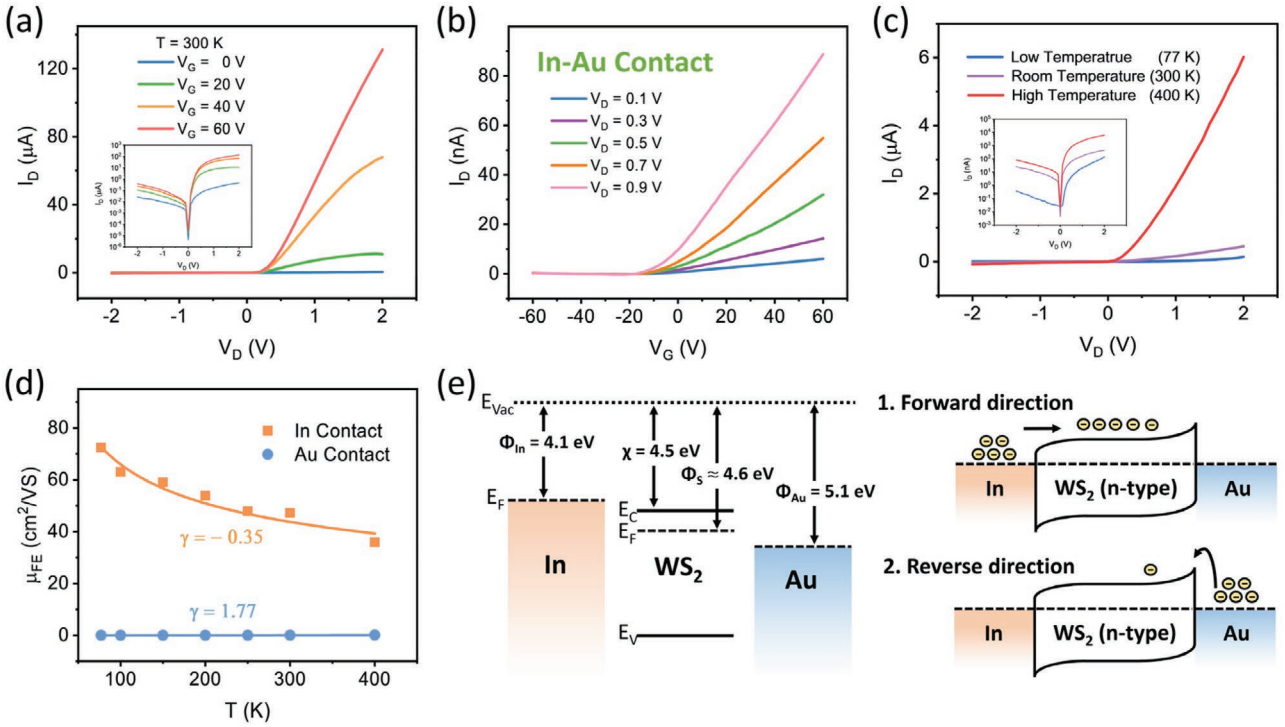

Figure 2. a) I_D–V_D characteristics of the WS_2 SBD with In–Au contacts depending on the different gate voltages showing diode characteristics at room temperature. Inset: Logarithmic scale of I_D–V_D characteristics at room temperature. b) I_D–V_G characteristics of the WS_2 SBD device at the different drain voltages. c) I_D–V_D characteristics of the WS_2 SBD device at low, room, and high temperatures. Inset: Logarithmic scale of I_D–V_D characteristics depending on the temperature. d) Variation in the mobility of In–In and Au–Au contacts for temperature in the range of 77–400 K. e) The band diagram of the WS_2 SBD in the forward direction with In contact showing Ohmic junction and the reverse direction with Au contact showing the Schottky junction with high SBH.

high as 3×10^2 at 77 K, showing the highest rectification ratio among all temperatures without the gate voltage (Figure S2a, Supporting Information). The measured diode current under a specific bias decreases as the temperature decreases in the forward and reverse bias regions.

Figure 3a,c shows the I_D–V_D characteristics of In–In and Au–Au contacts at different gate voltages. From the linear output characteristics, we can confirm that the In-In contacts form an Ohmic-like junction on WS_2 with low resistance. By contrast, Au–Au contacts exhibit nonlinear output characteristics, forming Schottky junctions with relatively high resistive contacts. Figure 3b,d shows the I_D–V_G characteristics of the In–In and Au–Au contacts depending on the drain voltages. The I_D–V_G characteristics of WS_2 with both contacts at different drain voltages showed excellent n-type properties. When n-type WS_2 is in contact with a higher work function metal ($\Phi_{Au} = 5.1$ eV), the electrons of the materials diffuse into the metal with a lower energy state owing to the difference in the Fermi level, and a depletion region is formed with the electric field. This phenomenon occurs until the Fermi level is aligned, and the electric field is included in the depletion region, which prevents the diffusion of electrons into the metal. This potential barrier in n-type WS_2, where the majority carrier is electrons, blocks flowing carriers showing Schottky junctions with Au, as shown in the schematic of Figure 3c. Conversely, when WS_2 is in contact with a metal with a small work function ($\Phi_{In} = 4.1$ eV) since the semiconductor has a smaller work function than the metal, electrons from the metal diffuse into the semiconductor during bonding, and the Fermi level is aligned.[25] In this case, the barrier in the conduction band region is very low, so electrons can more easily move from the WS_2 to the metal as shown in the schematic of Figure 3a.

The field-effect mobility (μ_{FE}) of WS_2 with In–In and Au–Au contacts was calculated as follows

$$\mu_{FE} = \frac{L}{W}\left(\frac{\partial I_D}{\partial V_G}\right)\frac{1}{C_{ox}\, V_D} \tag{1}$$

where L is the length of the device, W is the width of the device, I_D is the source drain current, V_G is the gate voltage, C_{OX} is the capacitance of 285 nm thick SiO_2, and V_D is the drain voltage. From the I_D–V_G curve of In–In and Au–Au contacts, $(\partial I_D/\partial V_G)$ can be extracted from the slope of the graph. The electron mobility of In–In contacts was found to be 47.2 $cm^2\ V^{-1}\ s^{-1}$ with a current on/off ratio of 10^7. By contrast, the electron mobility of Au–Au contacts was found to be 0.03 $cm^2\ V^{-1}\ s^{-1}$ with a current on/off ratio of 10^4 at room temperature. The on/off ratios of both contacts were extracted from the logarithm scale I_D–V_G curve shown in Figure S5a of the Supporting Information. These findings indicate that the electrical properties are improved when In makes contact with WS_2 instead of Au or Cr as shown in Figure S3 of the Supporting Information, which is due to the formation of Ohmic contacts and low work function metals. In addition, in Figure 2e, the contour of the energy band clearly shows that the Fermi level of In is shallower than that of WS_2.

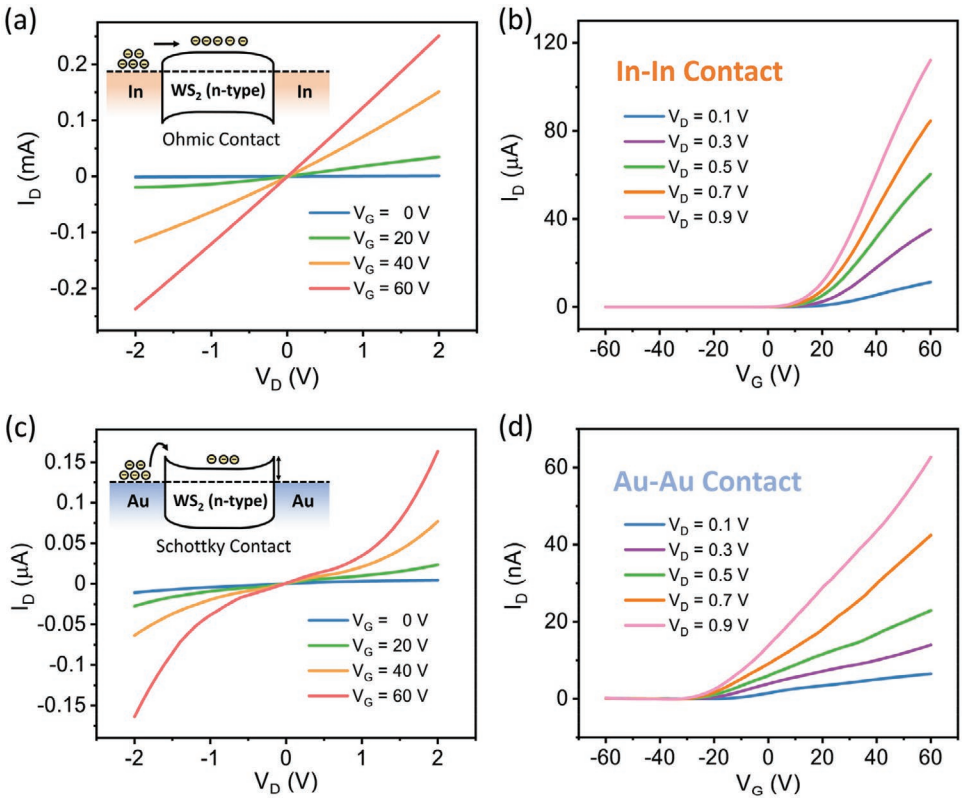

Figure 3. a) I_D–V_D characteristics of In–In contacts at the different gate voltages. Inset: Schematic diagram of In–In contacts showing Ohmic junction. b) I_D–V_G characteristics of In–In contacts at the different drain voltages. c) I_D–V_D characteristics of Au–Au contacts at the different gate voltages. Inset: Schematic diagram of Au–Au contacts showing Schottky junction. d) I_D–V_G characteristics of Au–Au contacts at the different drain voltages.

The field-effect mobility as a function of temperature T was also calculated from the I_D–V_G characteristics shown in Figure 2d and Figure S8 (Supporting Information). The dependence of mobility on temperature T can be described by the power-law $\mu_{FE} \approx T^{\gamma}$, which can directly represent the difference in the carrier transport mechanism. For the In–In, In–Au, and Au–Au contacts, the γ index values were found to be –0.35, –0.54, and 1.77, respectively (Figure 2d; Figure S8, Supporting Information). From the values, it can be clearly seen that the mobility of In–In and Au–Au contacts show reversal patterns as well as a strong and consistent dependence on temperature. With Au contacts, owing to the trapped charge impurity scattering, the electron mobility decreases with decreasing temperature. Conversely, with In contacts and In–Au contacts, the electron mobility increases with decreasing temperature, exhibiting a significant suppression of phonon scattering on electrons, and leading to improved carrier mobility.[29,30]

According to the thermionic emission theory, the current in the device can be obtained as follows

$$I = AA^{*}T^{3/2}\exp\left(-\frac{e\varnothing_B}{k_BT}\right)\exp\left(\frac{eV_D}{k_BT}-1\right) \quad (2)$$

where I is the current, A is the area of the device, A^* is the modified Richardson constant, $\varnothing_B$ is the SBH, V_D is the drain voltage, e is the electron charge, k_B is the Boltzmann constant, and T is the temperature in Kelvin.[31] To quantitatively evaluate the SBH in the device, we performed electrical characterization at different temperatures (77–400 K), as shown in Figure 5a,b displaying the transfer curves of each In–In and Au–Au contacts over a wide range of temperatures with the source to drain current on a logarithmic scale. To obtain an accurate $\varnothing_B$, the SBH $\varnothing_B$ needs to be determined at the flat band voltage condition ($V_{GS} = V_{FB}$) based on the thermionic emission theory equation. To obtain $\varnothing_B$, we plotted various values of ln ($I_D/T^{3/2}$) at a fixed drain bias of 0.1 V for various gate bias voltages as an Arrhenius plot. The slope of these lines directly provides the SBH $\varnothing_B$ (in eV) for the corresponding gate bias voltage, V_{GS}. For comparison, Arrhenius graphs are plotted for In–In and Au–Au contacts for all gate voltages, and the slope is plotted as a function of the gate voltage, as shown in **Figure 4**a,c. The Schottky barrier for V_{GS} less than or equal to V_{FB}, which was obtained from Figure 4b,d, linearly corresponds to V_{GS}, as shown in Figure 4b,d. However, as V_{GS} increases above V_{FB}, the plot deviates from its linear relationship. Hence, the accurate $\varnothing_B$ value obtained at a flat band voltage conditions for devices with the In–In contacts was 1.7 meV at flat band voltage V_{FB} = 8.4 V. Compared to this, the $\varnothing_B$ value of the Au–Au contacts was 34 meV at flat band voltage V_{FB} = 21.6 V, which is 20 times higher than that of the In–In contacts. Evidently, the SBH calculated according to the Schottky–Mott rule is due to the work function modulation of the metal, and much less disturbance occurs in the contact with In. However, the SBH cannot be simply determined from the difference between the Fermi level of the metal and the conduction band minimum of

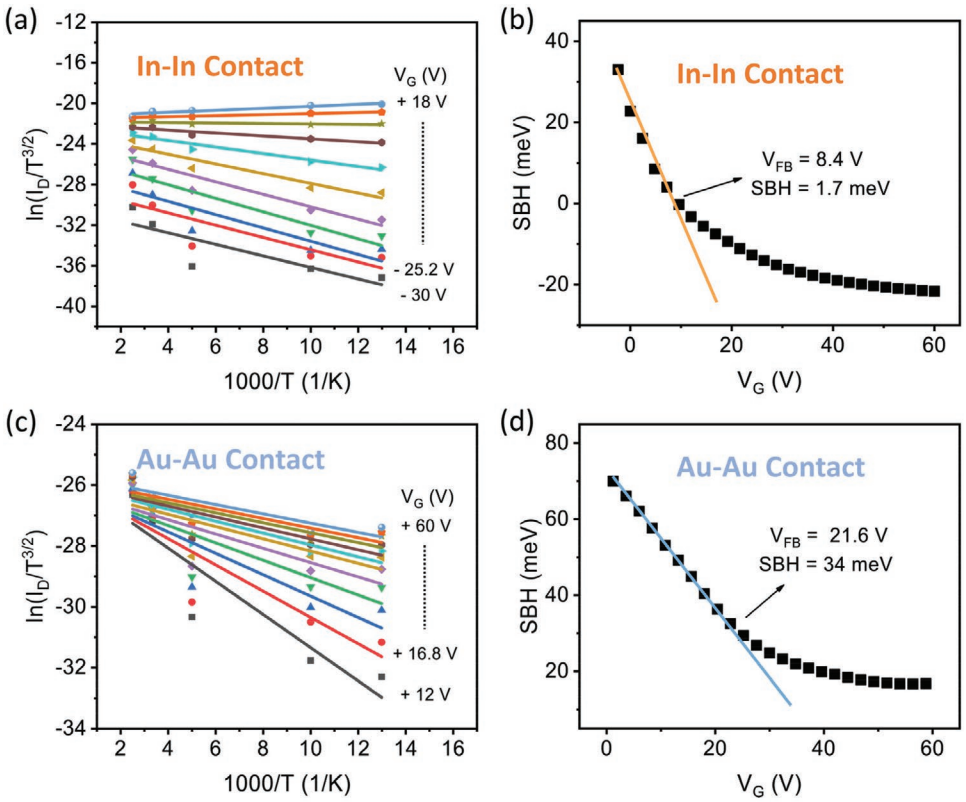

Figure 4. a) Arrhenius plot of the In-In contacts with ln ($I_D/T^{3/2}$) as a function of the gate voltage (V_G ranging from −30 to +18 V) observing the change in slope for different temperatures (77–400 K). b) SBH and flat-band voltage of the In–In contacts at the point when the slope changes depending on the gate voltage. c) Arrhenius plot of the Au–Au contacts with ln ($I_D/T^{3/2}$) as a function of the gate voltage (V_G ranging from +12 to +60 V) observing the change in slope at different temperatures (77–400 K). d) SBH and flat-band voltage of the Au–Au contacts at the point when the slope changes depending on the gate voltage.

the semiconductor. The potential difference between the metal and WS_2 calculated by the Schottky–Mott rule is different from the ideal value estimated by the band alignment of In–In and Au–Au contacts to WS_2. In general, when metal and TMD materials make contact, unlike bulk, the density of gap states caused by defects occurs on the interface of TMDs and metals, which is the main reason for Fermi level pinning. Owing to the interface states induced by In top contact evaporation, the Fermi level of In is pinned to a lower energy state. By contrast, there is no Fermi level pinning at the Au and WS_2 interface because the WS_2 was lightly transferred onto the Au bottom electrodes.[32,33] Despite the pinning effects, the potential barriers of the In and WS_2 contacts forming Ohmic-like contacts are smaller than those of Au and WS_2.

To estimate the rectifying performance of the WS_2 SBD device with different metal contacts, the ideality factor was calculated at the forward-biased region from a plot of the logarithmic output *I–V* characteristics shown in **Figure 5**c by fitting to the Shockley diode equation[34]

$$I = I_S\left[\exp\left(\frac{eV_D}{nk_BT} - 1\right)\right] \tag{3}$$

where I is the diode current, and I_S is the reverse saturation current defined as

$$I_S = AA^*T^2\exp\left(-\frac{e\varnothing_B}{k_BT}\right) \tag{4}$$

where V_D is the drain voltage, e is the electron charge, k_B is Boltzmann constant, T is the temperature in K, n is the ideality factor, A is the area of the diode, and $A^* = 4\pi qm^*k^2/h^3$ ($m^* = 0.34\ m_0$) is the effective Richardson constant.[2] The term "−1" is negligible under high applied drain voltages. To calculate the ideality factor n, take the logarithm of both sides and simplify the Shockley diode equation as follows

$$n = \frac{e}{k_BT\left\{\frac{d(\ln I)}{dV}\right\}} \tag{5}$$

Figure 5c shows the logarithm of the *I–V* curve at room temperature. The ideality factor of 1.02 is calculated using the slope of the logarithm *I–V* curve with a zero-gate voltage.

The ideality factor indicates how ideal the diode is. The closer the ideality factor is to 1, the more ideal the diode, and it increases as the current decreases. The ideality factor obtained from the slope of the *I–V* curve in the low current region without the back-gate voltage was 1.02, which is very close to 1. Given that the ideality factor is relative to the value of 1, the forward current largely depends on the diffusion of electrons and exhibits

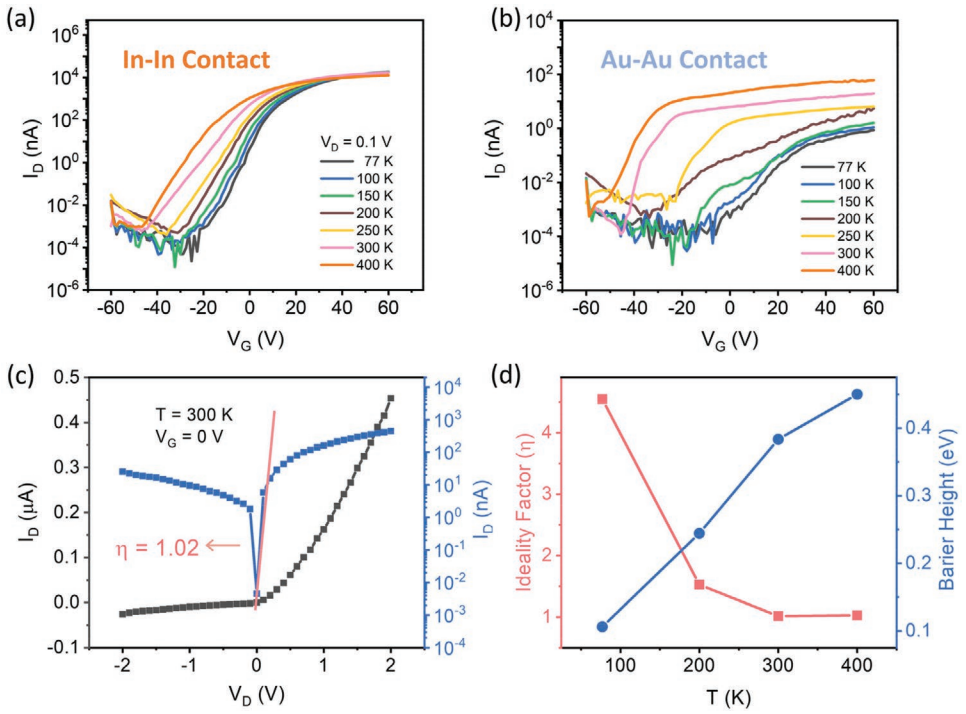

Figure 5. a) Temperature-dependent (77–400 K) I_D–V_G characteristics of the In contacts to WS_2 for gate voltages ranging from −60 to +60 V at a drain voltage of 0.1 V. b) Temperature-dependent (77–400 K) I_D–V_G characteristics of the Au contacts to WS_2 for gate voltages ranging from −60 to +60 V at a drain voltage of 0.1 V. c) The ideality factor of the WS_2 SBD device calculated from the slope at the low bias current region with a zero-gate voltage at room temperature. d) The ideality factor and barrier height of the WS_2 SBD device as a function of temperature.

ideal-like diode characteristics compared with the other group's reports[21,22,32,35,36] as detailed in **Table 1**. In addition, to confirm the characteristics of the diode based on the temperature and current transfer mechanism, it was measured from low temperature (77 K) and expressed based on temperature. The variation in the ideality factor with temperature (77–400 K) was calculated with the slope at the forward-biased region, as shown in Figure S6 of the Supporting Information. Figure 5d shows the variation in the ideality factor and barrier height of the WS_2 SBD with temperature. The barrier height was calculated from the reverse saturation current equation. As can be seen in Figure 5d, where as the ideality factor increases with decreasing temperature, barrier height decreases, showing a strong dependence on temperature. The current through the metal–semiconductor contact is a thermally assisted process, in which electrons solely can overcome the lower Schottky barrier at a lower temperature, resulting in a higher ideality factor. The discrepancy of ideality factor at 400 K showing nonideal dependence is due to several factors such as interface quality, surface defect density, and deposition process.[37,38] By contrast, as the temperature increases, electrons transfer through the higher barrier. This can be explained by the inhomogeneous barrier height.[39,40]

Table 1. Comparison of device characteristics with previously published reports using MoS_2 and $MoTe_2$.

Sample	Contact	Ideality factor
WS_2 SBD (our work)	In–Au contact	$n = 1.02$
$MoTe_2$ SBD[21]	Pd–Cr contact	$n = 1.4$
MoS_2 SBD[22]	Au–Cr contact	$n = 1.5$
MoS_2 SBD[31]	Ag–Pt contact (bottom contact)	$n = 1.09$
MoS_2 SBD[34]	Ti–Pt contact	$n = 1.55$
MoS_2 SBD[35]	Ag–Pt contact	$n = 2.1$

3. Conclusions

In summary, we developed the WS_2 SBD device without conventional p–n junction or doping. Depending on the work function, using In with low work function and Au with higher work function, asymmetric metal contacts exhibited excellent diode characteristics. In particular, an ideality factor of ≈1 was achieved for the WS_2 SBD with a simple structure. Compared to previous works, this value demonstrates the ideal-like diode characteristics without the junction that can, degrade the performance of the diode. The device also exhibited remarkable diode properties over a wide range of operating temperatures (77–400 K) with potential application to the preparation of future functional devices. We confirmed the electron transport mechanism of each metal contact with WS_2 by calculating the SBH, mobility, and on/off ratio as a function of temperature. It was verified that the In electrodes exhibit remarkably improved electrical properties compared to Au contacts.

4. Experimental Section

Fabrication of WS_2 Device: Bulk n-type WS_2 crystal (HQ graphene Inc.) was used for exfoliation on a precleaned and highly p-doped Si substrate

covered by a 285 nm thick SiO_2 layer using a conventional Scotch tape method. The few-layer flakes were then identified by optical microscopy. A suitable few-layer WS_2 was selected and stacked by the dry transfer method on the target Au electrodes, which were prepatterned on an empty Si/SiO_2 substrate using e-beam lithography techniques with In (10 nm)/Au (30 nm) deposition for Au contact in advance. To pick up the few-layer WS_2 flake, a polydimethylsiloxane base substrate covered by a polycarbonate (PC) sacrificial layer was used. Then, the WS_2 flake was deterministically released on the targeted Au electrodes in a glove box filled with argon gas. The residual PC was removed by immersing the sample in chloroform for 30 min, followed by drying using a nitrogen blow. After the transfer, In electrodes were patterned using e-beam lithography followed by metal deposition In (10 nm)/Au (30 nm) in an electron-beam deposition chamber and then annealed at 150 °C for 3 h in a high vacuum state (≈10^{-6} Torr).

Characterization of WS_2 Device: The thickness of the WS_2 flake was determined using AFM. Raman spectroscopy was performed to characterize the flakes using a 532 nm laser under ambient conditions. Electrical characterization of the device was performed under vacuum in a dark environment using a Keithley 4200-SCS parameter analyzer.

Supporting Information

Supporting Information is available from the Wiley Online Library or from the author.

Acknowledgements

This work was supported by the National Research Foundation of Korea (NRF) grant funded by the Korean government (MSIT) (No. 2019R1A2C2088719).

Conflict of Interest

The authors declare no conflict of interest.

Data Availability Statement

The data that support the findings of this study are available from the corresponding author upon reasonable request.

Keywords

metal–semiconductor junction, p–n diode, Schottky diode, work function, WS_2

Received: September 20, 2021
Revised: October 27, 2021
Published online:

[1] G. Fiori, F. Bonaccorso, G. Iannaccone, T. Palacios, D. Neumaier, A. Seabaugh, S. K. Banerjee, L. Colombo, *Nat. Nanotechnol.* **2014**, *9*, 768.
[2] D. Ovchinnikov, A. Allain, Y. S. Huang, D. Dumcenco, A. Kis, *ACS Nano* **2014**, *8*, 8174.
[3] Y. Cui, R. Xin, Z. Yu, Y. Pan, Z. Y. Ong, X. Wei, J. Wang, H. Nan, Z. Ni, Y. Wu, T. Chen, Y. Shi, B. Wang, G. Zhang, Y. W. Zhang, X. Wang, *Adv. Mater.* **2015**, *27*, 5230.
[4] M. Kang, B. Kim, S. H. Ryu, S. W. Jung, J. Kim, L. Moreschini, C. Jozwiak, E. Rotenberg, A. Bostwick, K. S. Kim, *Nano Lett.* **2017**, *17*, 1610.
[5] X. L. Li, W. P. Han, J. B. Wu, X. F. Qiao, J. Zhang, P. H. Tan, *Adv. Funct. Mater.* **2017**, *27*, 1604468.
[6] J. Kang, L. Zhang, S. H. Wei, *J. Phys. Chem. Lett.* **2016**, *7*, 597.
[7] C. Xia, W. Xiong, J. Du, T. Wang, Y. Peng, Z. Wei, J. Li, Y. Jia, *Small* **2018**, *14*, 1800365.
[8] S. Jo, N. Ubrig, H. Berger, A. B. Kuzmenko, A. F. Morpurgo, *Nano Lett.* **2014**, *14*, 2019.
[9] K. F. Mak, J. Shan, *Nat. Photonics* **2016**, *10*, 216.
[10] X. Y. Lin, W. Yang, K. L. Wang, W. S. Zhao, *Nat. Electron.* **2019**, *2*, 274.
[11] E. C. Ahn, *npj 2D Mater. Appl.* **2020**, *4*, 17.
[12] D. Zhong, K. L. Seyler, X. Linpeng, R. Cheng, N. Sivadas, B. Huang, E. Schmidgall, T. Taniguchi, K. Watanabe, M. A. McGuire, W. Yao, D. Xiao, K. C. Fu, X. Xu, *Sci. Adv.* **2017**, *3*, 1603113.
[13] F. Langer, C. P. Schmid, S. Schlauderer, M. Gmitra, J. Fabian, P. Nagler, C. Schuller, T. Korn, P. G. Hawkins, J. T. Steiner, U. Huttner, S. W. Koch, M. Kira, R. Huber, *Nature* **2018**, *557*, 76.
[14] A. Pospischil, M. M. Furchi, T. Mueller, *Nat. Nanotechnol.* **2014**, *9*, 257.
[15] K. Chen, X. Wan, J. Wen, W. Xie, Z. Kang, X. Zeng, H. Chen, J. B. Xu, *ACS Nano* **2015**, *9*, 9868.
[16] A. Pezeshki, S. H. Shokouh, T. Nazari, K. Oh, S. Im, *Adv. Mater.* **2016**, *28*, 3216.
[17] I. Lee, S. Rathi, D. Lim, L. Li, J. Park, Y. Lee, K. S. Yi, K. P. Dhakal, J. Kim, C. Lee, G. H. Lee, Y. D. Kim, J. Hone, S. J. Yun, D. H. Youn, G. H. Kim, *Adv. Mater.* **2016**, *28*, 9519.
[18] Y. Ding, N. Zhou, L. Gan, X. X. Yan, R. Z. Wu, I. H. Abidi, A. Waleed, J. Pan, X. W. Ou, Q. C. Zhang, M. H. Zhuang, P. Wang, X. Q. Pan, Z. Y. Fan, T. Y. Zhai, Z. T. Luo, *Nano Energy* **2018**, *49*, 200.
[19] Y. Kim, S. Lee, J. G. Song, K. Y. Ko, W. J. Woo, S. W. Lee, M. Park, H. Lee, Z. Lee, H. Choi, W. H. Kim, J. Park, H. Kim, *Adv. Funct. Mater.* **2020**, *30*, 2003360.
[20] M. Mathew, C. S. Rout, *J. Mater. Chem. C* **2021**, *9*, 395.
[21] J. Y. Wu, Y. T. Chun, S. Li, T. Zhang, D. Chu, *ACS Appl. Mater. Interfaces* **2018**, *10*, 24613.
[22] S. Aftab, M. W. Iqbal, A. M. Afzal, M. F. Khan, G. Hussain, H. S. Waheed, M. A. Kamran, *RSC Adv.* **2019**, *9*, 10017.
[23] J. Park, M. S. Kim, E. Cha, J. Kim, W. Choi, *Sci. Rep.* **2017**, *7*, 16121.
[24] A. Kuc, N. Zibouche, T. Heine, *Phys. Rev. B* **2011**, *83*, 245213.
[25] L. Zeng, L. Tao, C. Tang, B. Zhou, H. Long, Y. Chai, S. P. Lau, Y. H. Tsang, *Sci. Rep.* **2016**, *6*, 20343.
[26] D. S. Schulman, A. J. Arnold, S. Das, *Chem. Soc. Rev.* **2018**, *47*, 3037.
[27] F. Wang, I. A. Kinloch, D. Wolverson, R. Tenne, A. Zak, E. O'Connell, U. Bangert, R. J. Young, *2D Mater.* **2016**, *4*, 015007.
[28] A. Berkdemir, H. R. Gutierrez, A. R. Botello-Mendez, N. Perea-Lopez, A. L. Elias, C. I. Chia, B. Wang, V. H. Crespi, F. Lopez-Urias, J. C. Charlier, H. Terrones, M. Terrones, *Sci. Rep.* **2013**, *3*, 1755.
[29] Z. Y. Ong, M. V. Fischetti, *Phys. Rev. B* **2013**, *88*, 165316.
[30] S. Majdi, V. Djurberg, N. Suntornwipat, M. Gabrysch, J. Isberg, *Adv. Theory Simul.* **2020**, *4*, 2000103.
[31] J. Kim, A. Venkatesan, H. Kim, Y. Kim, D. Whang, G. H. Kim, *Adv. Sci.* **2021**, *8*, 2100102.
[32] Y. Liu, J. Guo, E. Zhu, L. Liao, S. J. Lee, M. Ding, I. Shakir, V. Gambin, Y. Huang, X. Duan, *Nature* **2018**, *557*, 696.
[33] K. Nassiri Nazif, A. Kumar, J. Hong, N. Lee, R. Islam, C. J. McClellan, O. Karni, J. van de Groep, T. F. Heinz, E. Pop, M. L. Brongersma, K. C. Saraswat, *Nano Lett.* **2021**, *21*, 3443.
[34] S. Aftab, M. F. Khan, P. Gautam, H. Noh, J. Eom, *Nanoscale* **2019**, *11*, 9518.
[35] Neetica, S. K. , A. Sanger, H. K. Chourasiya, A. Kumar, K. Asokam, R. Chandra, V. K. Malik, *J. Alloys Compd.* **2019**, *797*, 582.
[36] M. Moun, R. Singh, *Semicond. Sci. Technol.* **2018**, *33*, 125001.
[37] W. Jiang, T. Zheng, B. Wu, H. X. Jiao, X. D. Wang, Y. Chen, X. Y. Zhang, M. Peng, H. L. Wang, T. Lin, H. Shen, J. Ge, W. D. Hu, X. F. Xu, X. J. Meng, J. H. Chu, J. L. Wang, *Light: Sci. Appl.* **2020**, *9*, 160.
[38] C. P. Y. Wong, C. Troadec, A. T. S. Wee, K. E. J. Goh, *Phys. Rev. Appl.* **2020**, *14*, 054027.
[39] B. H. Moon, G. H. Han, H. Kim, H. Choi, J. J. Bae, J. Kim, Y. Jin, H. Y. Jeong, M. K. Joo, Y. H. Lee, S. C. Lim, *ACS Appl. Mater. Interfaces* **2017**, *9*, 11240.
[40] M. H. Ziko, A. Koel, T. Rang, M. H. Rashid, *Crystals* **2020**, *10*, 636.

